Hindawi
International Journal of Aerospace Engineering
Volume 2020, Article ID 6841651, 9 pages
https://doi.org/10.1155/2020/6841651

Research Article

Door-Triggering Mechanism for Large-Scale Rapid-Decompression Experiments

Lei Zhang,[1] **Xiao Han**,[1] **Xinbin Zhang**,[2] **and Jihong Yan**[2]

[1]*Beijing Institute of Spacecraft Environment Engineering, Beijing 100094, China*
[2]*Laboratory for Space Environment and Physical Sciences, Harbin Institute of Technology, Harbin 150001, China*

Correspondence should be addressed to Lei Zhang; zhangleicast@126.com

Received 8 August 2019; Revised 7 May 2020; Accepted 24 June 2020; Published 1 August 2020

Academic Editor: Antonio Viviani

For large-scale rapid-decompression experiments, a new door-triggering mechanism is proposed for a 750 mm diameter pressure relief channel. Quick opening of the door is realized by utilizing a spring-based release mechanism to instantly convert large amounts of elastic potential energy into kinetic energy. To counteract the significant inertial effect of the high-speed door on the chamber, a flywheel-based cushioning mechanism is designed to absorb the kinetic energy of the door after opening. This carefully designed mechanism consists of the closing mechanism, energy storage unit, locking/releasing mechanism, and cushioning mechanism. Kinetic models are established to analyze the dynamic properties. Simulation results reveal that it takes approximately 280 ms for the door to open from 0° to 90°. This work can provide insights for the development of large-scale rapid-decompression equipment in the future.

1. Introduction

Aircraft have greatly advanced the progress of human civilization by bringing people from different regions of the world closer to one another and have extended human activities to outer space. However, in the current aircraft industry, risks are still associated with the entire process from the departure of the aircraft to its landing. One of the most common problems that can inhibit the safe operation of an aircraft is the sudden loss of cabin pressure, which not only causes physical problems to human beings but also affects the properties and performance of airborne devices [1–10]. One of the most famous rapid-decompression accidents in history occurred with Soyuz 11 in 1971. While reentering the Earth's atmosphere, the pressure valve of the reentry capsule was accidentally opened due to mechanical failure, leading to a sudden loss of cabin pressure. Although the reentry capsule managed to return to the ground, three astronauts died due to decompression [11, 12].

A simulation study by Daidzic and Simones [8] showed that cabin decompression time is 7.8–78 s for a typical large aircraft and 0.2–1.8 s for a typical midsize one, which greatly depends on the rupture area. For cockpit decompression, the process is explosive and may occur within tens or hundreds of milliseconds. Even today, rapid-decompression accidents still occasionally occur, especially in civilian aircraft, causing casualties and economic losses [13–16]. For example, in 2018, the Sichuan Airlines Flight 3U8633 experienced an adventurous voyage. Approximately 30 min after the flight took off, the cockpit windshield cracked, accompanied by a rapid loss of pressure and drop in temperature. One pilot was sucked halfway out of the window and most of the equipment malfunctioned. Fortunately, the flight was successfully diverted via efficient maneuvering by the captain [13]. In the same year, three rapid-decompression accidents occurred with Southwest Airlines in one month, and many passengers were injured or killed [17]. Therefore, to improve aircraft safety, it is of great significance to develop rapid-decompression experiment techniques and study the effects of rapid decompression on human beings and airborne devices.

A sudden loss of cabin pressure is usually accompanied by shock waves, altitude hypoxia, low temperature, etc. On the one hand, people on board can suffer from severe physiological reactions. On the other hand, rapid decompression

can instantly generate large pressure differences on some airborne devices, especially sealed ones. It can also cause mechanical damage that leads to negative effects on heat dissipation, power output, lubrication failure, and electrical properties [18, 19]. Currently, in the Aviation Industry Standard HB 6167/6167A and National Military Standard GJB 150/150A of China, there are explicit provisions for rapid-decompression experiments: it should take no longer than 15 s for pressure to decrease from 75.2 to 18.8 kPa/4.4 kPa. The existing rapid-decompression equipment generally consists of an accessory chamber, main chamber, and valve. The accessory chamber is a low-pressure or vacuum vessel, and the main chamber is a normal-pressure vessel in which the samples are placed. When the valve is quickly opened, the air in the main chamber streams into the accessory chamber to simulate rapid decompression. However, relevant decompression equipment is only meant for small samples such as electronic components and instruments, and the volume is usually about 0.04 m^3 [20]. This is because the current valve cannot meet the requirements for a large-scale rapid-decompression environment. For large samples, the common method is to use a large-volume sealed vessel (such as a balloon) to hold the sample and place the vessel in a low-pressure chamber. Then, the vessel is punctured so the sample is instantly exposed to the rapid-decompression environment [18]. However, this method has some disadvantages: the sealed vessel is a solo unit associated with a high cost and long experimental period and the blasting process is too dangerous to use with people.

Considering the problems that exist in the current rapid-decompression experiment techniques, this work focused on designing a new mechanical door-triggering mechanism for large-scale rapid-decompression equipment. The mechanism is found to demonstrate features such as easy control, high reliability, reusability, and high test efficiency. Section 2 describes the entire design philosophy. Section 3 discusses the structural designs and analyses of the closing mechanism, energy storage unit, releasing mechanism, and cushioning mechanism. Finally, the findings of this work are summarized in Section 4.

2. Design Principle of Door-Triggering Mechanism

For large-scale rapid-decompression equipment, a large pressure relief channel is required to minimize the time required for the pressure relief process. The valve or door should be large enough and should open in a short time, indicating that the door-triggering mechanism has the ability to instantly output a large amount of energy. For common motors or hydraulic drivers, high actuating speed and output force cannot be simultaneously realized; thus, a spring is utilized to store and release a large amount of energy so the door can open quickly. Figure 1 shows the schematic of a large-scale rapid-decompression equipment, which mainly consists of the door-triggering mechanism, low-pressure chamber (18.8 kPa), pressure relief channel, and sample chamber (75.2 kPa). The sample chamber and low-pressure chamber are connected by the pressure relief channel, and the door-triggering mechanism is in the low-pressure chamber. The opening direction of the chamber door is toward the side of the low-pressure chamber. The differential pressure on both sides of the chamber door can facilitate quick opening of the door, and a higher differential pressure leads to a higher opening speed. To ensure that the door can be quickly opened in a limited time under different pressure difference conditions, the initial pressure difference in this study is set to zero, which represents the worst case. Therefore, for a certain pressure difference in the test, the actual opening time of the door will be lower than the design value in this study. The focus of this work is to achieve a quick opening of the door in a limited time. Because of the initial condition of zero pressure difference, the volumes of the low-pressure chamber and the sample chamber are not within the scope of this study.

As shown in Figure 1, the door-triggering mechanism is composed of the closing mechanism, energy storage unit, locking/releasing mechanism, and cushioning mechanism. The closing mechanism uses the connecting rod hold-down mechanism, which is driven by motors via a ball screw. To reduce the rotational inertia of the door and the motion decoupling, the hold-down mechanism is separated from the door. When closing the door, the spring is gradually compressed and elastic energy is gradually stored in the energy storage unit. The releasing mechanism is used to quickly release the door. Considering that the high-speed door can exert a large inertial impact on the chamber, a cushioning mechanism is designed for absorption of kinetic energy of the door after opening.

Before the test, the door and the locking/releasing mechanism are all set to the open state, and the energy storage unit is in the unstored state. During the test, the operation steps of the door-triggering mechanism are summarized as follows:

(1) After the sample is placed in the sample chamber, the door closing mechanism pushes the door to rotate and close. In the latter stage of closing, the door contacts the energy storage unit and compresses the spring to store energy. The door closing mechanism stops when the door is closed

(2) When the locking/releasing mechanism starts to operate, it pushes the connecting rod mechanism to rotate to a given position to lock the door

(3) Then, the motor of the door closing mechanism is reversed and the connecting rod and the door are separated to move to given positions

(4) After establishment of the test environment, the pendulum of the locking/releasing mechanism is released when the door is opened, and the gravitational potential energy is converted into kinetic energy to impact the slider to quickly release the holding unit of the connecting rod to the hatch. Then, the energy storage unit instantly releases energy to push the door open

(5) After the door is fully opened, it begins to contact the buffer mechanism, which absorbs the rotational kinetic energy of the door with the help of the inertia flywheel

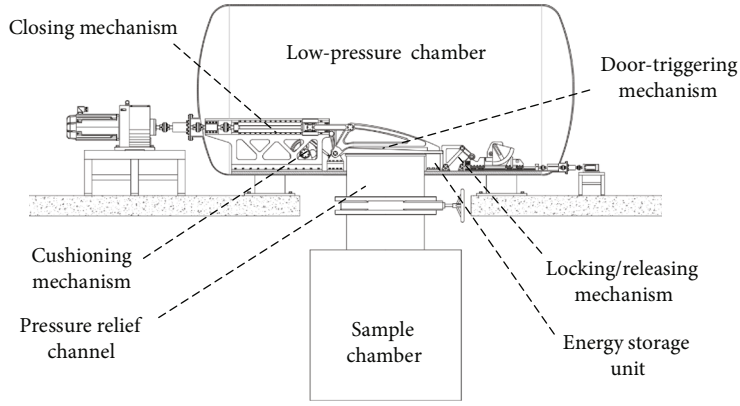

Figure 1: Schematic of the large-scale rapid-decompression equipment.

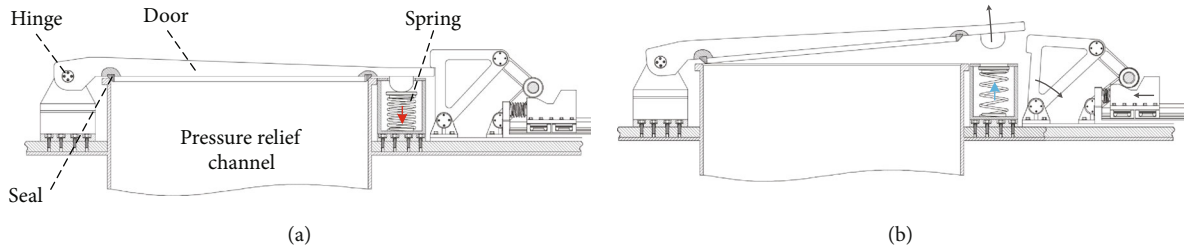

Figure 2: Computer-assisted design (CAD) model of the spring-based energy storage unit: (a) energy storage state and (b) energy release state.

3. Structural Design and Analysis

3.1. Energy Storage Unit. The spring-based energy storage unit provides a large amount of energy for the door to open quickly, as shown in Figure 2. When the door closing mechanism pushes the door closed, the spring is compressed to store energy. The state of energy storage is shown in Figure 2(a). When the locking/releasing mechanism is opened, the chamber door is released and a large amount of stored energy is released by the spring to quickly push the chamber door open. The state of energy release can be found in Figure 2(b). The opening process of the door can be divided into two stages: the accelerating stage and the uniform motion stage. In the design, the hinge adopts a rolling bearing; therefore, its friction coefficient is small and can be ignored here. In addition, to ensure that the opening time of the designed mechanism will not be adversely affected by the pressure difference, the opening direction of the chamber door is toward the side of the low-pressure chamber, so the greater the pressure difference, the shorter the actual opening time of the chamber door. In this simulation, the most unfavorable initial condition is adopted, that is, the pressure difference is 0. Considering that the air density at 18.8 kPa is relatively low, by ignoring the air resistance in the accelerating stage, the motion of the door can be described by

$$k_e b\left(2\alpha_0\alpha_x - \alpha_x^{\,2}\right) - I\dot{\alpha}_x^{\,2} = 0, \tag{1}$$

where k_e is the elastic coefficient of the spring, b is the distance between the door hinge and the spring-door contact point, α_0 denotes the door rotation angle when the spring is in the maximum compression state, α_x is the door rotation angle, and I is the rotational inertia of the door around the hinge. In Equation (1), the first term on the left represents the elastic potential energy released by the spring and the second term represents the rotational kinetic energy of the door. The time needed for the door to open t_e can be expressed as

$$t_e = \int_0^{\alpha_t} \frac{1}{\dot{\alpha}_x} \mathrm{d}\alpha + \frac{\alpha_e - \alpha_t}{w_t}, \tag{2}$$

where w_t is the maximum rotation speed and α_e and α_t are, respectively, the maximum rotation angle of the uniform motion stage and the accelerating stage that satisfy the following geometrical conditions:

$$\begin{cases} (1 - e_k)l = c + b\tan\alpha_t, \\ b\tan\alpha_0 = l - c, \end{cases} \tag{3}$$

where e_k is the ratio of tight deformation in advance, l is the free length of the spring, and c denotes the spring length when the door is closed.

For a pressure relief channel 750 mm in diameter, the door weighs approximately 120 kg, and the rotational inertia around the hinge is approximately 43 kg·m^2. Here, b, c, e_k, and α_e are 980 mm, 150 mm, 10%, and 90°, respectively. Assuming that the door can be opened in 300 ms with four springs, the rotation angle α_t during the accelerating stage can be related to the elastic coefficient k_e by solving

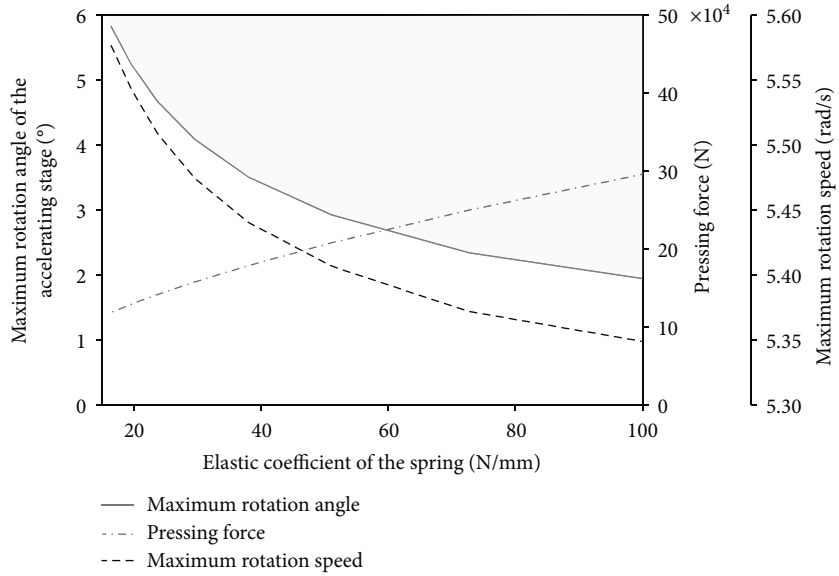

Figure 3: Relationship between the maximum rotation angle of the accelerating stage and the elastic coefficient.

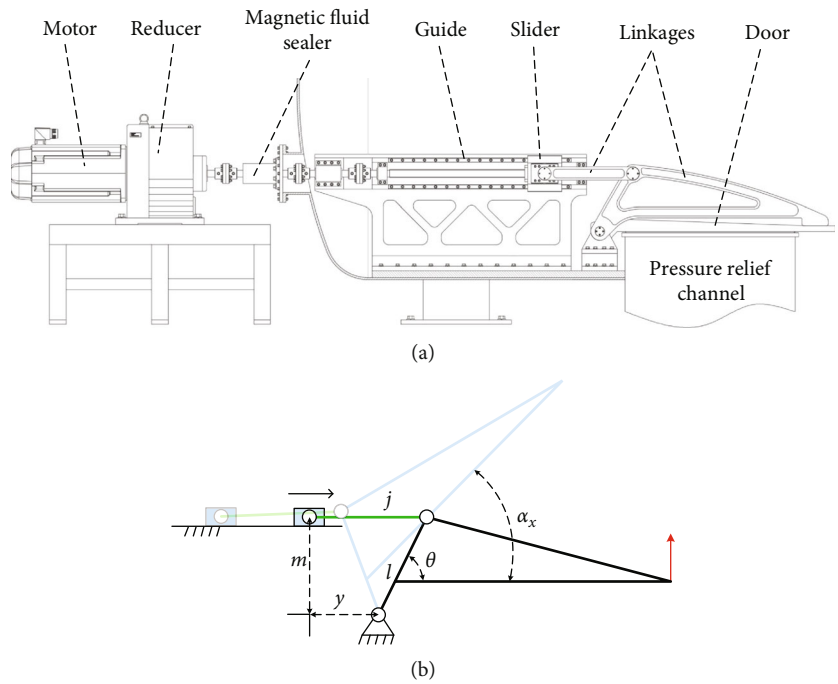

Figure 4: Schematic of the crank-sliding closing mechanism: (a) CAD model and (b) analysis model.

Equations (1)–(3). Figure 3 shows the numerical results with the help of ADAMS software, which is a widely used commercial software dealing with multibody system dynamic problems. It can be seen that the rotation angle α_t declines with k_e, and only in the dash area where α_t and k_e lie can t_e be less than 300 ms. The smaller the k_e, the lower the pressing force. However, as k_e decreases, the required maximum rotation speed increases, generating larger impacts on the chamber. Based on these considerations, the elastic coefficient k_e is set to 30 N/mm and the corresponding α_t is 4°.

3.2. Closing Mechanism. To reduce the mass and moment of inertia of the door, the door closing mechanism and the door are considered to be two independent units. When the door is closed, the door closing mechanism can push it tightly closed. After the locking/releasing mechanism locks the door, the door closing mechanism and the door are separated. When closing the door, the closing mechanism experiences a maximum spring force of 30×10^4 N. As shown in Figure 4(a), a crank-sliding mechanism is adopted to constitute the closing mechanism; it is composed of linkages, a slider, and a guide.

The guide is driven by a motor outside the chamber with a magnetic fluid sealer.

Figure 4(b) shows the analysis model of the crank-sliding closing mechanism in which l, θ, h, j, and m are structural parameters and $\alpha_x \in [0, \alpha_e]$. Then, the rotation angle α_x must satisfy

$$\alpha_x = \tan^{-1}\left(\frac{y}{m}\right) + \frac{\pi}{2} - \cos^{-1}\left(\frac{y^2 + m^2 + l^2 - j^2}{2\sqrt{l(y^2 + m^2)}}\right), \quad (4)$$

where y is the displacement of the slider.

During the locking process when $\alpha_x \in [0, \alpha_e]$, the closing mechanism presses the spring to store energy. Considering that the locking process is very slow, by neglecting the effects of the inertial force, the thrust for pushing the slider F can be determined by the following equation:

$$Fl\frac{\sin(\theta + \alpha_x)}{1 + c\tan\gamma} = bk(\alpha_0 - \alpha_x), \quad (5)$$

where c is the friction coefficient of the slider and γ is the angle between linkage j and the horizontal direction. γ can be expressed by

$$\gamma = \cos^{-1}\left(\frac{j^2 + m^2 + y^2 - l^2}{2j\sqrt{m^2 + y^2}}\right) - \tan^{-1}\left(\frac{m}{y}\right). \quad (6)$$

Equation (5) indicates that during the spring-compressing process, increasing $l\sin\theta$ and using smaller c and γ can contribute to the reduction of the thrust F. The effects of the structural parameters on thrust F were analyzed in detail. Figure 5 shows the numerical results. It can be seen that with the increase in j, the rotation angle changes little, while the required thrust force increases significantly. The larger the θ, the higher the rotation angle and the thrust force. When θ is below 45°, the rotation angle can reach 90°. m plays a negative role in the rotation angle while playing a positive role in the required thrust force. Accordingly, θ, j, and m are set to 60°, 0.4 m, and 0.25 m, respectively.

3.3. Locking/Releasing Mechanism. When the door is completely closed, it should be locked before the closing mechanism is separated from it. The locking force is the sum of the spring force and the pressure difference. Here, the locking function is realized by combining a plane four-bar linkage and a linear slider with a fixed wedge. Between the linkage and the wedge, a roller is used to reduce friction. As shown in Figure 6(a), the linear slider is driven by a motor outside the chamber by a magnetic fluid sealer. A ball screw is used to convert the rotation to a straight movement. When releasing the door, a pendulum-like mechanism is designed to strike the wedge to move it by converting a large amount of gravitational potential energy into kinetic energy to instantly release the door. This is to overcome the high friction between the roller and wedge. The working process of the pendulum is shown in Figure 6(b). The sliding block is initially located on the right side of the pendulum. However, when the door needs to be opened, it moves to the left to push the pendulum up, then moves to the left side of the pendulum, and finally, the pendulum returns to its original position. The sliding block slides in the reverse direction to push the pendulum up, then the pendulum breaks away from the slide, and the free-falling body impacts the wedge to release the door.

Figure 6(b) shows the analysis model of the locking/releasing mechanism in which l_1, l_2, l_3, and l_4 are the lengths of the four-bar linkage and β_1, β_2, β_3, and β_4 are the corresponding rotation angles. When pushing the wedge, two types of friction forces can be found: one is exerted on the wedge and the other acts on the slider from the guide. Assuming that the integrated friction coefficient is c_1, then, neglecting the effects of inertial force, the thrust required to overcome the friction force F_l can be expressed as

$$F_l = \frac{d_1(\tan\beta_1\tan(\theta_1 - \beta_3) + 1)}{l_1 + l_4\cos\beta_1(\tan\beta_1\tan(\theta_1 - \beta_3) + 1)}c_1F_t, \quad (7)$$

where d_1 is the horizontal displacement between the action point of the locking force and the spindle of l_2 and F_t denotes the locking force. As can be seen in Equation (7), smaller d_1 and c_1 can lead to larger l_1 and l_4. Here, c_1, d_1, l_1, and l_4 are set to 0.1, 30, 165, and 135 mm, respectively. With $\beta_1 = 45°$, the thrust reaches a minimum value of 30 N when $\theta_1 - \beta_3$ is −45°. Here, the masses of the wedge and pendulum are 1 kg and 10 kg, respectively, and the radius of the pendulum is 150 mm. Given that the wedge needs to move 10 mm to release the door, according to the conservation of energy, it takes about 2 ms to enable the mechanism to release the door instantly.

3.4. Cushioning Mechanism. To counteract the high inertial impact of the high-speed door on the chamber, a flywheel-based cushioning mechanism is designed to absorb the kinetic energy of the door after opening, as shown in Figure 7. The mechanism is mainly composed of the rod, a parallel four-bar mechanism, tension spring, flywheel, torsional spring, and electromagnetic transducer. The electromagnetic transducer is positioned outside the chamber and connected with the flywheel via a magnetic fluid sealer. A one-way bearing can be found between the four-bar mechanism and the flywheel. When the door rotates to 90° and contacts the rod, the rod starts to drive the four-bar mechanism to rotate by a torsional spring. Meanwhile, the flywheel starts to rotate and gradually absorbs the kinetic energy of the door, and a small amount of energy is converted into the elastic potential energy of the tension spring. Then, the flywheel is slowed down by the electromagnetic transducer to convert the kinetic energy into electric energy.

Figure 7(b) shows the analysis model in which I_1, I_2, and I_3 are the rotational inertias of the relevant rods and k_1 and k_2 are the elastic coefficients of the torsional spring and tension spring, respectively. In the design, the hinge adopts a rolling bearing whose friction coefficient is relatively small. By ignoring the energy loss caused by friction,

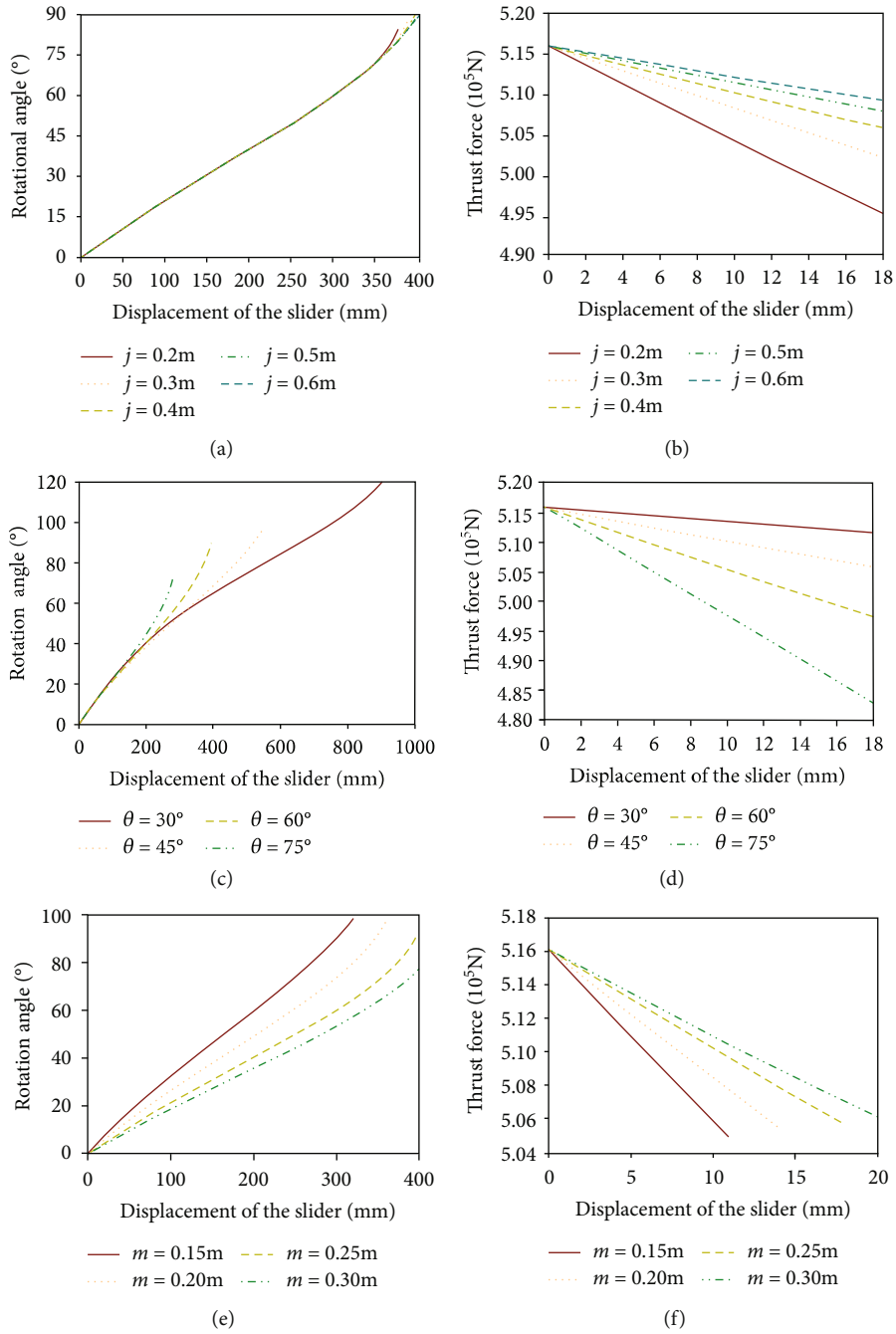

Figure 5: Effects of structural parameters on rotation angle and thrust force.

according to the conservation of energy and momentum, we can obtain

$$\begin{cases} Iw_0^2 = I\dot{\alpha}_x^2 + I_1\dot{\alpha}_1^2 + I_2\dot{\alpha}_2^2 + I_3\dot{\alpha}_3^2 + k_1(\alpha_2 - \alpha_1)^2 + k_2(d_2 - d_j)^2, \\ Iw_0 = I\dot{\alpha}_x + I_1\dot{\alpha}_1 + I_2\dot{\alpha}_2 + I_3\dot{\alpha}_3, \end{cases} \tag{8}$$

where α_i ($i = x$, 1, 2, and 3) denotes the rotation angle of the door, rods, and flywheel; w_0 is the maximum rotation speed of the door; and d_j and d_2 are the initial and actual lengths of the diagonal, respectively. In Equation (8), the first formula is for energy conservation. The left term of the equation represents the kinetic energy before the collision between the door and the buffer mechanism, which can be gradually converted into the rotational kinetic energy of the door, rod 1, rod 2, and rod 3 and the elastic potential energy of springs k_1 and k_2 (i.e., the first, second, third, fourth, fifth, and sixth terms on the right side of the equation). The second formula of Equation (8) is for momentum conservation. The term on the left side of the equation indicates the momentum before the collision between the door and the buffer mechanism. It is gradually converted into the momentum of the door, rod 1,

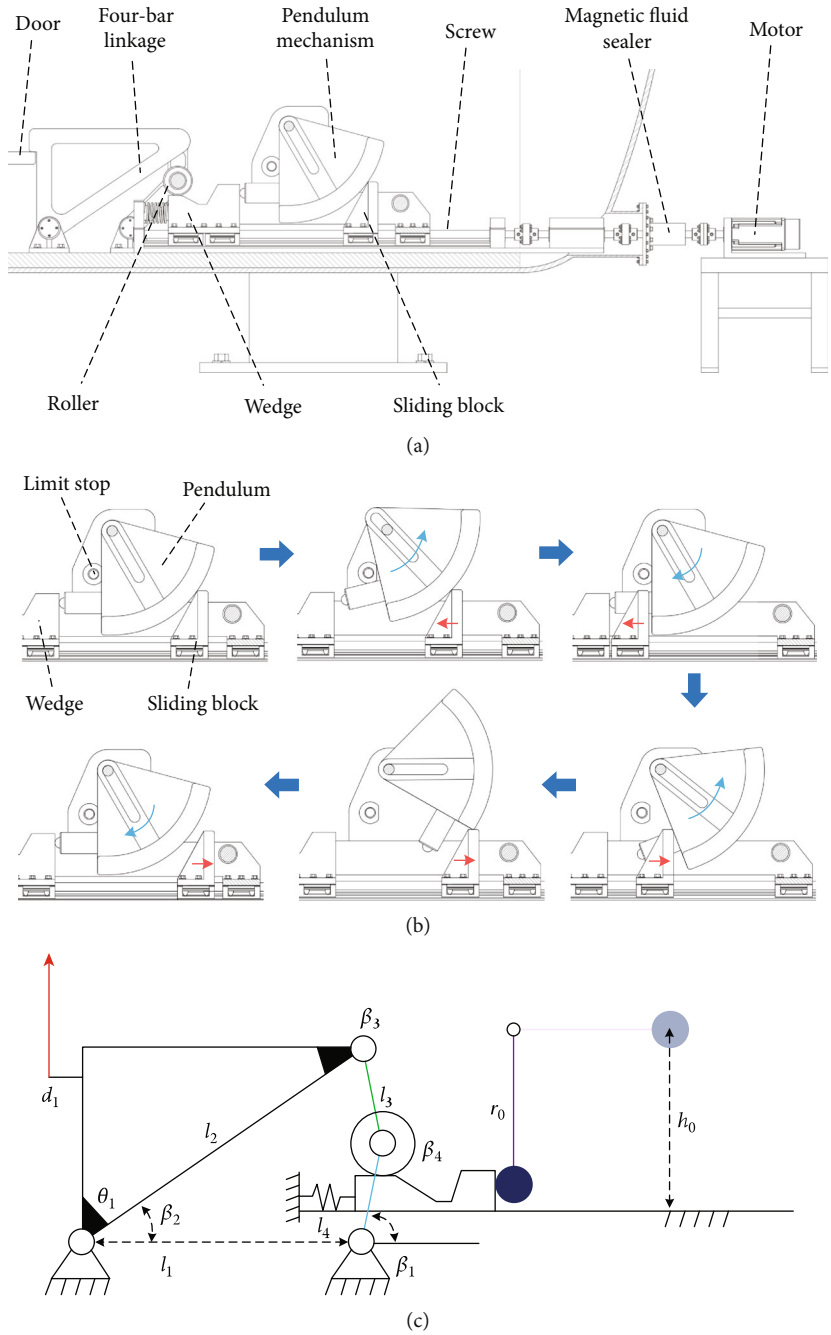

Figure 6: Schematic of the locking/releasing mechanism: (a) CAD model, (b) releasing process, and (c) analysis model.

rod 2, and rod 3 (i.e., the first, second, third, and fourth terms on the right side of the equation). We can obtain

$$\begin{cases} d_2 = \sqrt{l_5^2 + l_6^2 - 2l_5 l_6 \cos(\alpha_x + \alpha_e)}, \\ d_j = \sqrt{l_5^2 + l_6^2 - 2l_5 l_6 \cos \alpha_e}. \end{cases} \quad (9)$$

In this work, the final designed k_1, k_2, I_1, and I_3 are set to 1 N/mm, 2 N/mm, 1.25 kg·m^2, and 20 kg·m^2, respectively, and I_2 is ignored as it is small compared to I_3. Then, with the help of ADAMS, the dynamic properties of the mechanism can be numerically revealed. Figure 8 shows the characteristic curve of the buffer mechanism. It can be seen that it takes about 280 ms for the door to rotate from 0° to 90°. Figure 9 shows the resistance moment of inertia of the flywheel from the opening of the door to the end of the buffer. When the door rotates to near 90°, the cushioning mechanism starts to work and provides a large resistance moment to slow down the rotation speed of the door. With the cushioning mechanism, the speed of the door quickly decreases to zero, indicating that the designed cushioning mechanism is suitable for counteracting the great inertial effect of the

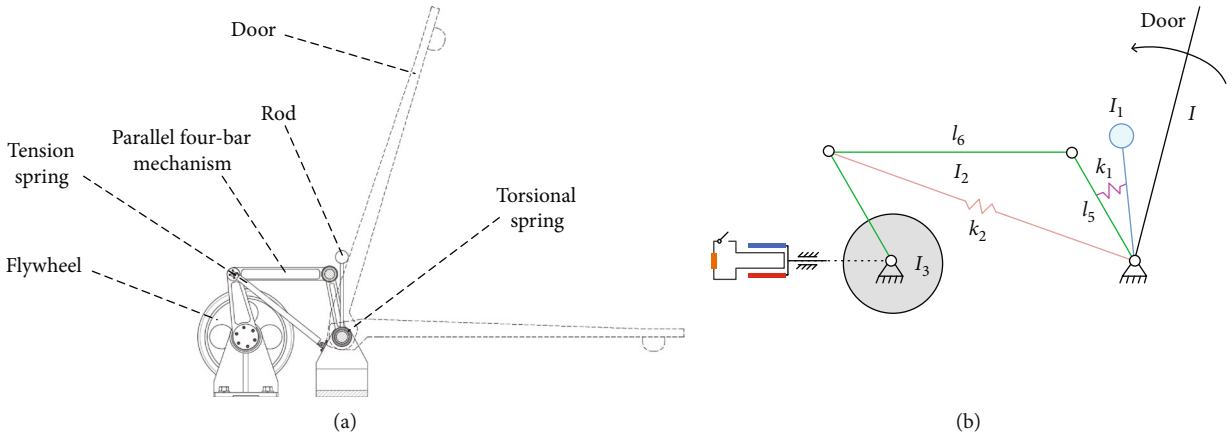

Figure 7: Schematic of the cushioning mechanism: (a) CAD model and (b) analysis model.

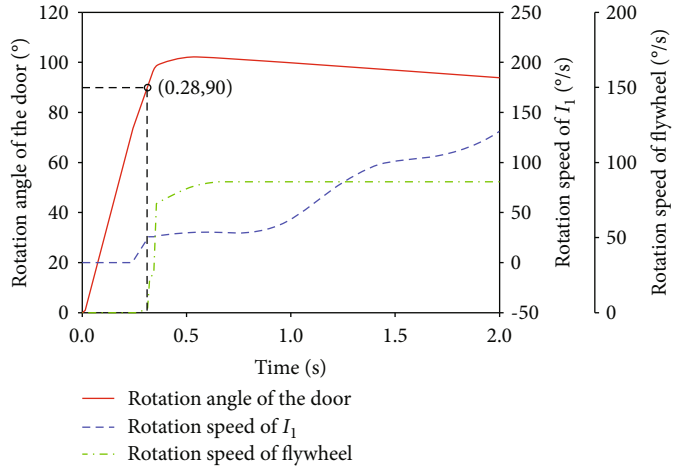

Figure 8: Dynamic properties of the buffer mechanism.

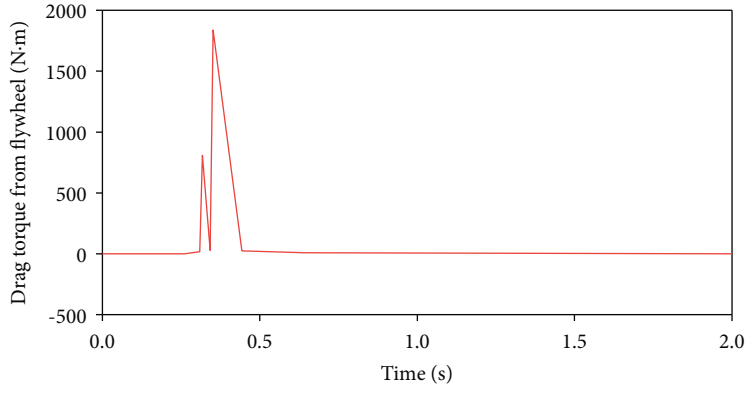

Figure 9: Drag torque from the flywheel.

high-speed door on the chamber. According to Ref. [14], for a typical two-compartment-cabin system with a sudden breach of 0.5 m^2, the decompression time from 78.959 kPa to 19.74 kPa is numerically calculated to be approximately 1.8 s. These initial conditions are quite similar to the design conditions of this work, so the designed door-triggering mechanism is qualified to carry out large-scale rapid-decompression experiments.

4. Conclusions

In this work, a new mechanical door-triggering mechanism is proposed for large-scale rapid-decompression experiments. The mechanism is composed of the closing mechanism, energy storage unit, locking/releasing mechanism, and cushioning mechanism. The energy storage unit uses springs to provide a large amount of energy for the door to open

instantly. The crank-sliding mechanism is utilized to constitute the closing mechanism that exerts a large output force to close the door and presses the springs to store energy. The locking/releasing mechanism can lock the door by overcoming the large resultant force of the spring force and pressure difference. It can also release the door in 2 ms by combining a plane four-bar linkage, a wedge, and a pendulum-like mechanism. The cushioning mechanism uses a flywheel to absorb the large kinetic energy of the door to counteract the large inertial effect of the high-speed door on the chamber. In addition, kinetic models are established and the effects of the structural parameters on the dynamical properties are studied. It is found that the designed door-triggering mechanism for a 750 mm pressure relief channel is capable of opening the door from 0° to 90° within 280 ms, which is suitable for rapid-decompression experiments. This new mechanism can be used to develop large-scale rapid-decompression equipment in the future.

Data Availability

The data used to support the findings of this study are available from the corresponding author upon request.

Conflicts of Interest

There are no conflicts of interest to declare.

Acknowledgments

The authors acknowledge the financial support provided by the Science and Technology on Reliability and Environmental Engineering Laboratory of BISEE Foundation (Project No. CAST-BISEE2017-017).

References

[1] S. Demetriades, "On the decompression of a punctured pressurized cabin in vacuum flight," *Jet Propulsion*, vol. 24, no. 1, pp. 35-36, 1954.

[2] R. Bancroft, "Pressure cabins and rapid decompression," *Aerospace Medicine*, pp. 337–363, 1971.

[3] H. Marotte, C. Toure, J. Clere, and H. Vieillefond, "Rapid decompression of a transport aircraft cabin: protection against hypoxia," *Aviation, Space, and Environmental Medicine*, vol. 61, no. 1, pp. 21–27, 1990.

[4] G. Cable, "In-flight hypoxia incidents in military aircraft: causes and implications for training," *Aviation, Space, and Environmental Medicine*, vol. 74, no. 2, pp. 169–172, 2003.

[5] C. Hackworth, L. Peterson, D. Jack, and C. Williams, "Altitude training experiences and perspectives: survey of 67 professional pilots," *Aviation, Space, and Environmental Medicine*, vol. 76, no. 4, pp. 392–394, 2005.

[6] A. Macmillan, "Principles of the pressure cabin and the effects of pressure change on body cavities containing gas," in *Ernsting's Aviation Medicine*, pp. 109–127, Hodder Arnold, London, 4 edition, 2006.

[7] J. Auten, M. Kuhne, H. Walker, and H. Porter, "Neurologic decompression sickness following cabin pressure fluctuations at high altitude," *Aviation, Space, and Environmental Medicine*, vol. 81, no. 4, pp. 427–430, 2010.

[8] N. E. Daidzic and M. P. Simones, "Aircraft decompression with installed cockpit security door," *Journal of Aircraft*, vol. 47, no. 2, pp. 490–504, 2010.

[9] H. Han, Z. Zhu, and C. Liu, "Protective principles and protection equipment for aircrew during flight under the condition of low," *China Personal Protection Equipment*, vol. 4, pp. 49–53, 2016.

[10] N. E. Daidzic, "An algebraic model of high-altitude aircraft decompression and emergency descent," *Aviation*, vol. 21, no. 3, pp. 92–101, 2017.

[11] C. Moening, "Pyrotechnic shock flight failures," in *IES Pyrotechnic Shock Tutorial Program, 31st Annual Technical Meeting*, Institute of Environmental Sciences, 1985.

[12] N. J. Szewczyk and W. McLamb, "Surviving atmospheric spacecraft breakup," *Wilderness & Environmental Medicine*, vol. 16, no. 1, pp. 27–32, 2005.

[13] J. Bai, X. Chen, J. Yang, and S. Yang, "Simulation of aircraft cabin pressure loss," *Journal of Civil Aviation University of China*, vol. 32, no. 6, pp. 1–6, 2014.

[14] A. Pagani and E. Carrera, "Gasdynamics of rapid and explosive decompressions of pressurized aircraft including active venting," *Advances in Aircraft and Spacecraft Science*, vol. 3, no. 1, pp. 77–93, 2016.

[15] R. Bason and D. Yacavone, "Loss of cabin pressurization in US naval aircraft: 1969-90," *Aviation, Space, and Environmental Medicine*, vol. 63, no. 5, pp. 341–345, 1992.

[16] S. L. Jersey, G. L. Hundemer, R. P. Stuart, K. N. West, R. S. Michaelson, and A. A. Pilmanis, "Neurological altitude decompression sickness among U-2 pilots: 2002–2009," *Aviation, Space, and Environmental Medicine*, vol. 82, no. 7, pp. 673–682, 2011.

[17] http://news.21cn.com/domestic/yaowen/a/2018/0515/10/32919255.shtml.

[18] http://baijiahao.baidu.com/s?id=1600416866258725410&wfr=spider&for=pc.

[19] X. Song and B. Zhuo, "Low pressure test standard and test technical analysis," *Environmental Technology*, vol. 6, pp. 94–97, 2014.

[20] X. Su, "Research on rapid decompression testing technologies for airborne equipment," *Environmental Technology*, vol. 33, no. 2, pp. 18–22, 2011.